

Enhancing Interaction Modeling with Agent Selection and Physical Coefficient for Trajectory Prediction

Shiji Huang, Lei Ye, Min Chen, Wenhai Luo, Dihong Wang, Chenqi Xu, Deyuan Liang

Abstract—A thorough understanding of the interaction between the target agent and surrounding agents is a prerequisite for accurate trajectory prediction. Although many methods have been explored, they all assign correlation coefficients to surrounding agents in a purely learning-based manner. In this study, we present ASPILin, which manually selects interacting agents and calculates their correlations instead of attention scores. Surprisingly, these simple modifications can significantly improve prediction performance and substantially reduce computational costs. Additionally, ASPILin models the interacting agents at each past time step separately, rather than only modeling the interacting agents at the current time step. This clarifies the causal chain of the target agent’s historical trajectory and helps the model better understand dynamic interactions. We intentionally simplified our model in other aspects, such as map encoding. Remarkably, experiments conducted on the INTERACTION, highD, and CitySim datasets demonstrate that our method is efficient and straightforward, outperforming other state-of-the-art methods.

I. INTRODUCTION

The ability to accurately forecast the trajectories of human-driven vehicles and pedestrians sharing the environment with autonomous vehicles is paramount within autonomous driving. Such precise trajectory predictions are indispensable for downstream intelligent planning systems to make informed decisions, thereby improving autonomous driving operations’ safety, comfort, and efficiency. However, due to the inherent uncertainty and the multi-modal nature of driving behaviors, vehicle trajectory prediction against an urban setting presents significant challenges that include, but are not limited to, spatio-temporal modeling of historical trajectories [1], interaction modeling [2], [3], environmental description [4], kinematic constraints [3], [5], and real-time inference [6].

Recent studies [2], [3], [7]–[9] focus on modeling interactions between agents, as it is a crucial element in autonomous driving. For instance, HiVT [7] and QCNet [9] leverage the attention mechanism to model agent-agent interactions, which can implicitly select significant nearby agents for the target agent. The larger attention weights indicate the importance of these agents. Although the results of these studies demonstrate the superiority of their interaction modeling, they still have some shortcomings:

(i) *Previous methods tend to take all surrounding agents as input to the interaction module.* However, human attention capacity is limited. In dynamic environments, one person can

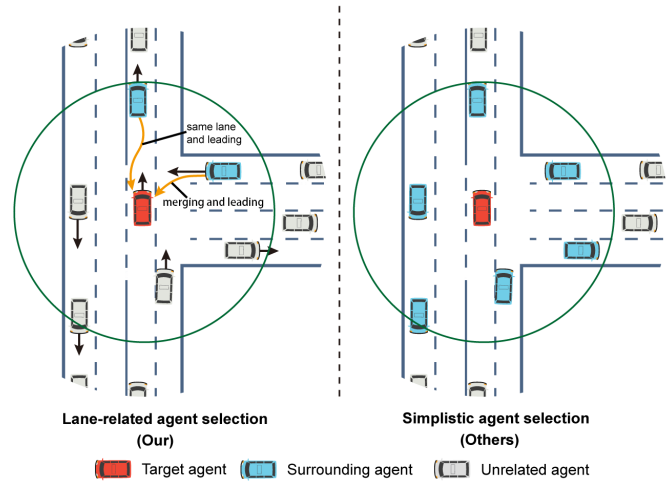


Fig. 1. Left: We first predict each agent’s future lane. Then, combine it with their current lane and direction relative to the target agent to select interacting agents further. Right: Classical agent selection method, which takes all agents within a defined range as model input.

focus on at most 5 agents at a time [10], meaning a huge amount of irrelevant agents are also input into the model, which significantly increases the model’s inference latency and may also reduce prediction performance, especially in interaction-rich scenarios.

(ii) *The interpretability of interaction encoding is low.* Attention mechanism [1] and Graph Neural Network (GNN) [11] are popular in numerous interaction-aware methods. Fundamentally, these methods do not elucidate the underlying decision logic or cognitive processes. Although recent methods [3], [5], [12] use a combination of physics- and learning-based approaches, their interaction encoding remains purely learning-based.

To this end, we present ASPILin, a simple Conditional Variational Autoencoder (CVAE) framework that utilizes reparameterization to predict future trajectories. For the interaction module, firstly, we introduce a more refined scheme for agent selection as illustrated in Fig. 1. However, a new challenge arises as well: if we, like most approaches [11]–[13], only model the interacting agents of the target agent at the current moment, early interacting agents may be ignored, leading to an incomplete causal chain of the entire trajectory. Thus, we perform agent selection at each historical moment and retain only their states at that moment, then concatenate the states from all moments to create a complete interaction representation. Lastly, we derive a novel correlation coefficient by estimating agents’ future nearest position, the

S. Huang, L. Ye, M. Chen, W. Luo, D. Wang, C. Xu, D. Liang are with the College of Computer Science and Technology, Zhejiang University of Technology, China (email: {shiji, yelei, cm, whailuo, wangdh, xucq, liangdy}@zjut.edu.cn). Corresponding author: Lei Ye.

time needed to reach that, and their current distance. All correlation coefficients are then normalized across the spatio-temporal dimensions to replace attention scores and are integrated into the Transformer framework. We deliberately used simple network structures to simplify our model for the other two modules (historical trajectory encoding and map encoding). Comparative experiments on the INTERACTION [14] and highD [15] datasets demonstrate that ASPILin is highly competitive with other state-of-the-art methods. More importantly, ablation studies on the INTERACTION and CitySim [16] datasets indicate that our improvements to the interaction module achieved better prediction performance with lower inference latency. We also highlight that these improvement strategies can be easily incorporated into other models, particularly the agent selection strategy.

II. RELATED WORK

A. Interaction-Aware Trajectory Prediction

Existing interaction-aware methods can be further explored from the perspectives of agent selection and interaction encoding.

For interacting agent selection, some methods [17], [18] directly model interactions with all agents within the scene and simultaneously predict the trajectories of multiple target agents. By contrast, setting a range threshold [1]–[4], [11], [13], [19] or limiting the maximum number of neighbors [8] permits modeling of the target agent’s local context, which aligns more closely with the needs of single-agent prediction [1], [4], [13]. Moreover, many works [1], [7], [8] conduct joint predictions by initially capturing local interactions before modeling global interactions, enabling the model to extend from single-agent prediction to multi-agent prediction. Most of these methods only model the interacting agents of the target agent at the current moment. For multi-step prediction methods [3] and vectorized representation methods [4], [7], they must model the interactions for each historical timestep.

For interaction encoding, all studies use purely learning-based approaches. However, in other respects, recent studies combine physics- and learning-based approaches, offering insights into improving model performance. SSP-ASP [5] and ITRA [3] limit motion learning to an action space grounded in acceleration and steering angles, subsequently deducing future trajectories via a kinematic model. M2I [12] classifies a pair of agents as influencer and reactor by calculating the closest value of their ground-truth trajectories and the time required to reach the nearest point at the training stage, followed by the sequential generation of their future trajectories via a marginal predictor and a conditional predictor, respectively.

B. Multi-modal Trajectory Prediction

The future trajectory of vehicles inherently exhibits multimodality, given the uncertainty of intentions. To tackle this challenge, one widely used approach involves modeling the output as a probability distribution of future trajectories via regression [7]. Usually, it introduces a cross-entropy loss

function for mode classification to avoid mode collapse. Some methods use more explicit classification representations to make multi-modal trajectories closer to reality. TNT [20] samples anchor points from the roadmap and then generates trajectories based on these anchors. SSL-Lanes [19] classifies the maneuvers of each agent and trains the model in a self-supervised manner.

Other methods parameterize the distribution of future trajectories [21], such as Gaussian Mixture Models (GMM) or samples within a latent space, and generate predictions through mapping. Regarding the latter, Generative Adversarial Networks (GANs) [22], Conditional Variational Autoencoders (CVAEs) [1], [23], and diffusion model [6] are the most popular models. A common drawback of generative models is the need for extensive data to support training. Moreover, for GANs, challenges such as training difficulties and mode collapse exist. For the diffusion model, multi-step denoising leads to significant computational overhead and high inference latency. Although CVAEs face issues of insufficient diversity like GANs, their training is more stable. In this study, instead of sampling randomly from a standard normal distribution, we treat the sampler as a trainable module to prevent unrealistic trajectory outputs due to randomness.

III. METHODOLOGY

A. Problem Formulation

Single-agent trajectory prediction is designed to forecast the future trajectory of a target agent conditioned on agents’ historical states X and the map information \mathcal{M} . To be more specific, we assume that at time t , there are N agents (vehicles, pedestrians, cyclists) in the scene, so their historical states can be represented as $X_t = [x_t^1, x_t^2, \dots, x_t^N] \in \mathbb{R}^{N \times 7}$, where x_t^n is the state of agent n at time t , including xy coordinates ($p_t^n \in \mathbb{R}^2$), heading angle ($h_t^n \in \mathbb{R}$), speed ($v_t^n \in \mathbb{R}^2$), and acceleration ($a_t^n \in \mathbb{R}^2$). Specifically, x_t^1 represents the state of the target agent at time t . Taking into account T_h historical observation timesteps, the overall historical state of the agents is denoted as $X = [X_{-T_h+1}, X_{-T_h+2}, \dots, X_0] \in \mathbb{R}^{N \times T_h \times 7}$. Similarly, the future ground-truth trajectory of the target agent is defined as $Y = [y_1, y_2, \dots, y_{T_f}] \in \mathbb{R}^{T_f \times 2}$ over T_f timesteps, where y_t is the xy coordinates at time t . To forecast multi-modal future trajectories, the predicted trajectory of K modes is denoted as $\hat{Y} = [\hat{Y}^1, \hat{Y}^2, \dots, \hat{Y}^K] \in \mathbb{R}^{K \times T_f \times 2}$. Our goal is to learn a generative model to parameterize the distribution $\mathcal{P}(Y|X, \mathcal{M})$.

B. Prediction Model

We named our proposed model ASPILin, emphasizing agent selection, physical interactions, and linear time weighting. An overview of our proposed ASPILin is illustrated in Fig. 2.

1) *Interacting agent selection*: We define the Euclidean distance between agent i and the target agent at time t as d_t^i . If d_t^i falls below a manually defined selection threshold \mathcal{D} , it

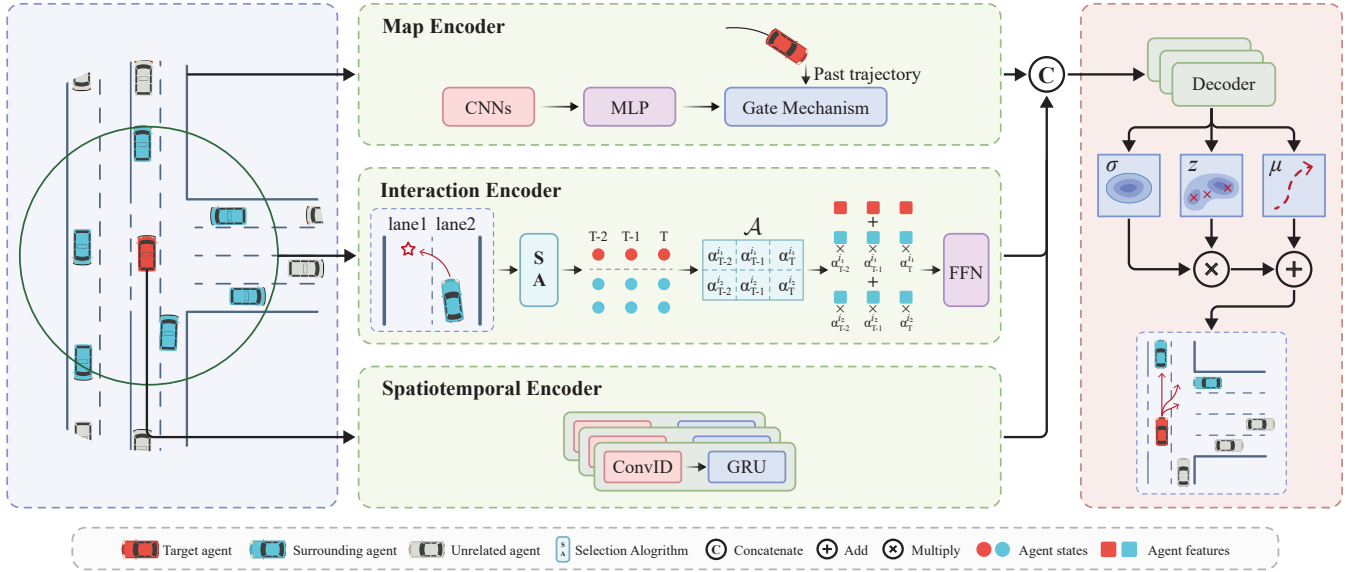


Fig. 2. The illustration of ASPILin. We focus on interaction modeling and deliberately simplify the design of other modules to prove the effectiveness of our method. A lane predictor and a new algorithm are used to select interacting agents further, and a novel physical correlation coefficient is designed to replace data-driven attention encoding. The multimodal trajectory prediction results are finally derived from a reparameterization formula.

is considered that there is a potential for interaction between agent i and the target agent.

In urban areas, vehicles operate within lanes while driving, which allows us to convert the problem of interaction between agents into a correlation problem between lanes. At time t , the lane to which agent i belongs is defined as l_t^i . As time passes, the agent will move to another lane, which we refer to as future lane l_{t+}^i ($t+ \leq T_f$). Because the size of each scene is finite, if l_t^i represents the last lane traversed by agent n in the scene, then it is stipulated that $l_{t+}^i = l_t^i$. The future lane l_{t+}^i can be easily captured for training data. However, a lane predictor must be built at the inference stage to predict l_{t+}^i . Intuitively, predicting the future lane can easily be converted into a classification problem. Nevertheless, this method is unsuitable for real-world applications as it only accommodates predictions in scenarios with training. For this purpose, we design an ultra-lightweight model Lin to forecast unimodal medium-to-high-precision trajectories for future moments, then map each timestep's trajectory onto the respective lane. Lin is a simplified version of ASPILin, which excludes the interaction module. The entire process can be expressed as $\{l_k^i\}_{k=-T_h+1}^0 = g(f_{\text{reg}}(\{\{x_k^i\}_{k=-T_h+1}^0, \mathcal{M}\}))$, where g is the mapping from trajectory to lane. One challenge of using this regression method is that agents in a real-world scenario sometimes have different observation steps. Yet, the model must predict the trajectories of all agents to ensure the accuracy of the interacting agent selection. Therefore, during inference, we use a Constant Acceleration model $\text{CA}(\cdot)$ to pad the missing observation steps for agents. For an agent i whose states $\{x_k^i\}_{k=t_1}^{t_2}$ ($-T_h+1 < t_1 \leq t_2 < 0$) are missing observation steps, the most recent state is used as the input for $\text{CA}(\cdot)$:

$$\{x_k^i\}_{k=-T_h+1}^{t_1-1} = \text{CA}(x_{t_1}^i), \quad (1)$$

$$\{x_k^i\}_{k=t_2+1}^0 = \text{CA}(x_{t_2}^i). \quad (2)$$

Then we select four different types of interacting agents as described in Alg. 1: *Same lane and Leading (SL)*, *Future*

Algorithm 1 Interacting agent selection algorithm

Input: Agents' state $X_t \in \mathbb{R}^{N \times 7}$, Agents' current and future lanes $L_t \in \mathbb{R}^{N \times 2}$, Selection threshold \mathcal{D}

Output: Index list \mathcal{N}

- 1: Extract position P_t and velocity V_t from X_t ;
 - 2: Initialize min-distance $d_{\text{SL}}, d_{\text{FL}}, d_{\text{FF}}, d_{\text{ML}} \leftarrow \mathcal{D}$;
 - 3: Initialize neighbor index list $\mathcal{N} \leftarrow [0, 0, 0, 0]$;
 - 4: **for** each agent $i \leftarrow 2$ **to** N **do**
 - 5: Distance $d_t^i \leftarrow \|p_t^i - p_t^1\|_2$;
 - 6: Orientation $o_t^i \leftarrow (p_t^i - p_t^1) \cdot v_t^1$;
 - 7: **if** $d_t^i < d_{\text{SL}}$ and $l_t^i = l_t^1$ and $o_t^i \geq 0$ **then**
 - 8: $d_{\text{SL}} \leftarrow d_t^i$;
 - 9: $\mathcal{N}[0] \leftarrow i$;
 - 10: **else if** $d_t^i < d_{\text{FL}}$ and $l_t^i = l_{t+}^1$ and $o_t^i \geq 0$ and $l_{t+}^1 \neq l_t^1$ **then**
 - 11: $d_{\text{FL}} \leftarrow d_t^i$;
 - 12: $\mathcal{N}[1] \leftarrow i$;
 - 13: **else if** $d_t^i < d_{\text{FF}}$ and $l_t^i = l_{t+}^1$ and $o_t^i < 0$ and $l_{t+}^1 \neq l_t^1$ **then**
 - 14: $d_{\text{FF}} \leftarrow d_t^i$;
 - 15: $\mathcal{N}[2] \leftarrow i$;
 - 16: **else if** $d_t^i < d_{\text{ML}}$ and $l_t^i = l_{t+}^1$ and $o_t^i \geq 0$ and $l_{t+}^1 \neq l_t^1$ **then**
 - 17: $d_{\text{ML}} \leftarrow d_t^i$;
 - 18: $\mathcal{N}[3] \leftarrow i$;
 - 19: **end if**
 - 20: **end for**
 - 21: **return** \mathcal{N} ;
-

lane and Leading (FL), Future lane and Following (FF), and Merging and Leading (ML). If the angle between an agent's position relative to the target agent and the target agent's heading does not exceed 90° , this agent is considered leading the target agent. Each type's agent closest to the target agent is finally selected as its interacting agent.

2) *Interaction Representation*: Once the method for interacting agent selection is established, the next step is to create an interaction representation to serve as the input for the interaction encoder. A common practice is to select four types interacting agents i_1 to i_4 for the target agent at $t = 0$, denoted as $I = [\{x_k^1\}_{k=-T_h+1}^0, \{\{x_k^{i_n}\}_{k=-T_h+1}^0\}_{n=1}^4}] \in \mathbb{R}^{5 \times T_h \times 7}$. Our method is to choose four types of interacting agents for the target agent at every historical moment, defined as $I = [I^1, (I^s)_{s \in \mathcal{S}}] \in \mathbb{R}^{5 \times T_h \times 7}$, where $I^s = [x_{-T_h+1}^s, x_{-T_h+2}^s, \dots, x_0^s] \in \mathbb{R}^{T_h \times 7}$ represents the states of type s agents in all observation timesteps and $\mathcal{S} = \{\text{SL}, \text{FL}, \text{FF}, \text{ML}\}$. Both methods use the same spatial resources.

Similar to recent studies [2], [7], [11], we convert the coordinate system for the final interaction representation. Specifically, all states in I are transformed into a relative coordinate system as \tilde{I} with the target agent's final observation point p_0^1 as the origin and the positive direction h_0^1 of the x-axis.

3) *Interaction Encoding*: For the traditional multi-head dot-product attention mechanism, the interaction embedding e_{int} between the target agent and all of its interacting agents can be denoted as:

$$Z = \text{FC}(\tilde{I}) = [Z^1, (Z^s)_{s \in \mathcal{S}}], \quad (3)$$

$$Q, K, V = W^q Z^1, W^k (Z^s)_{s \in \mathcal{S}}, W^v (Z^s)_{s \in \mathcal{S}}, \quad (4)$$

$$Z' = \text{MHA}(Q, K, V), \quad (5)$$

$$e_{int} = \text{LN}(\text{FFN}(\text{LN}(Z^1 + Z')) + Z), \quad (6)$$

where $\text{FC}(\cdot) \in \mathbb{R}^{7T_h \times d_z}$ performs a direct linear transformation on the temporal dimension features, and Q, K, V are obtained from three equivalent linear transformations ($W^q, W^k, W^v \in \mathbb{R}^{d_z \times d_{z'}}$). Residual connection and layer normalization $\text{LN}(\cdot)$ are applied to the output Z from $\text{MHA}(\cdot)$ before input into the feed-forward module $\text{FFN}(\cdot)$, following the standard Transformer architecture.

We now introduce a physical method to calculate the correlation $\alpha_t^{i_1}$ between agent i_1 and the target agent at time t . First, we use the $\text{CA}(\cdot)$ to estimate the time $\tau_t^{i_1}$ needed for the target agent and agent i_1 to reach the closest distance $d_{t+}^{i_1}$, expressed as:

$$\tau_t^{i_1} = \arg \min_{\tau} \|\text{CA}(\tilde{x}_t^1) - \text{CA}(\tilde{x}_t^{i_1})\|_2, \quad (7)$$

$$d_{t+}^{i_1} = \|\text{CA}(\tilde{x}_t^1) - \text{CA}(\tilde{x}_t^{i_1})\|_2. \quad (8)$$

Then, combining with the current distance $d_t^{i_1}$ to calculate the correlation coefficient :

$$\bar{\tau}_t^{i_1} = \begin{cases} 0 & \text{if } \tau_t^{i_1} < 0; \\ T & \text{if } \tau_t^{i_1} > T; \\ \tau_t^{i_1} & \text{otherwise,} \end{cases} \quad (9)$$

$$c_t^{i_1} = \frac{d_t^{i_1} - d_{t+}^{i_1} + \epsilon}{d_t^{i_1} \exp(\bar{\tau}_t^{i_1})}. \quad (10)$$

Here, we set a lower bound for $\tau_t^{i_1}$ to ensure that the correlation coefficient is based solely on future action and an upper bound based on the assumption that agents will not stay in the scene for more than T seconds, to prevent excessively high values in subsequent calculations. Eq. 10 indicates that the correlation between agents is negatively correlated with $d_t^{i_1}$ and $\tau_t^{i_1}$, and positively correlated with the difference in the distance they cover during $\tau_t^{i_1}$. Adding an extra term ϵ in the numerator prevents it from 0, thereby maintaining the effectiveness of the two factors in the denominator. Using $\exp(\cdot)$ in the denominator serves to highlight the impact of $\tau_t^{i_1}$ and avoid the denominator being 0. If at time t there is no SL type agent i_1 , then $c_t^{i_1}$ is set to 0. Next, $c_t^{i_1}$ is normalized to a physical attention score:

$$\alpha_t^{i_1} = \alpha_t^{\text{SL}} = \frac{2(T_h + t)c_t^{i_1}}{(1 + T_h)T_h \sum_{n=1}^4 c_t^{i_n}}, \quad (11)$$

where $\alpha_t^{i_1}$ simultaneously incorporates the spatial attention of the target agent towards agent i_1 at time t and the linear weighting of t over the entire time scale T_h . Subsequently, we derive a weight matrix $\mathcal{A} \in \mathbb{R}^{4 \times T_h}$:

$$\mathcal{A} = \begin{bmatrix} \alpha_{-T_h+1}^{\text{SL}} & \cdots & \alpha_0^{\text{SL}} \\ \alpha_{-T_h+1}^{\text{FL}} & \cdots & \alpha_0^{\text{FL}} \\ \alpha_{-T_h+1}^{\text{FF}} & \cdots & \alpha_0^{\text{FF}} \\ \alpha_{-T_h+1}^{\text{ML}} & \cdots & \alpha_0^{\text{ML}} \end{bmatrix} = \begin{bmatrix} \mathcal{A}^{\text{SL}} \\ \mathcal{A}^{\text{FL}} \\ \mathcal{A}^{\text{FF}} \\ \mathcal{A}^{\text{ML}} \end{bmatrix}. \quad (12)$$

Ultimately, e_{int} is obtained by applying residual connection and layer norm:

$$Z = \text{FC}_z(\tilde{I}) = [Z^1, (Z^s)_{s \in \mathcal{S}}], \quad (13)$$

$$Z' = \text{FC}_{z'} \left(Z^1 + \sum_{s \in \mathcal{S}} \mathcal{A}^s \circ Z^s \right), \quad (14)$$

$$e_{int} = \text{FFN-LN}(\text{FFN}(\text{LN}(Z'))) + Z', \quad (15)$$

where $\text{FC}_z(\cdot) \in \mathbb{R}^{7 \times d_z}$ and $\text{FC}_{z'}(\cdot) \in \mathbb{R}^{d_z T_h \times d_{z'}}$ perform linear transformations on spatial and temporal features respectively, \circ denotes the Hadamard product. Inspired by NormFormer [24], we additionally use a LN placed after the FNN(\cdot) but before the residual connection on top of the Pre-LN configuration, referred to as $\text{FFN-LN}(\cdot)$, which helps enhance training stability.

4) *Spatiotemporal Encoder*: 1D Convolutional Neural Networks $\text{Conv1D}(\cdot)$ and Gated Recurrent Units $\text{GRU}(\cdot)$ are used to capture the spatial and temporal dependencies of the target agent's historical states in the relative coordinate system, ultimately resulting in a spatiotemporal embedding e_{st} :

$$e_{st} = \text{GRU}(\text{Conv1D}(\{\tilde{x}_k^1\}_{k=-T_h+1}^0)). \quad (16)$$

We use three equivalent but independent spatiotemporal encoders corresponding to decoders to obtain the mean μ , variance σ , and samples z used for reparameterization respectively. The corresponding embeddings are labeled as e_{st}^μ , e_{st}^σ , and e_{st}^z .

5) *Map Encoder*: The map selector from HEAT-I-R [2] is utilized as our map encoder. The entire process is as follows:

$$\mathcal{M}' = \text{MLP}(\text{CNNs}(\mathcal{M})), \quad (17)$$

$$x' = \text{FC}_{x'}(x_0^1), \quad (18)$$

$$e_{map} = \text{Sigmoid}(\text{FC}_m([\mathcal{M}', x'])) \circ \mathcal{M}'. \quad (19)$$

CNNs(\cdot) and MLP(\cdot) are utilized to extract features from the map and perform a linear transformation $\text{FC}_{x'}(\cdot) \in \mathbb{R}^{7 \times d_{x'}}$ of the target agent's state at the current time from global coordinates into a higher-dimensional space. Then, we fuse the features of x' and \mathcal{M}' ($\text{FC}_m(\cdot) \in \mathbb{R}^{(d_{x'} + d_{\mathcal{M}'}) \times d_{\mathcal{M}'}}$), pass them through Sigmoid(\cdot) to scale all feature values between 0 and 1, and finally perform element-wise production with \mathcal{M}' to obtain the map embedding e_{map} .

6) *Decoder and Reparameterization*: The mean and variance of the future trajectory of the target agent are forecasted at first, denoted as:

$$\mu = \text{MLP}_\mu([e_{st}^\mu, e_{int}, e_{map}]), \quad (20)$$

$$\sigma = \text{MLP}_\sigma([e_{st}^\sigma, e_{int}, e_{map}]), \quad (21)$$

where $\mu \in \mathbb{R}^{T_f \times 2}$ represents a set containing the means of the trajectory for each future timestep, and $\sigma \in \mathbb{R}$ is a single value. Next, we perform a set of linear transformations on the predicted σ and use it for sample prediction:

$$\sigma' = \text{MLP}_{\sigma'}(\sigma), \quad (22)$$

$$z = \text{MLP}_z([e_{st}^z, e_{int}, e_{map}, \sigma']), \quad (23)$$

where $z \in \mathbb{R}^{K \times T_f \times 2}$ represents the K samples for each future timestep. The predicted trajectory \hat{Y} is ultimately derived from a reparameterization formula:

$$\hat{Y} = \mu + \sigma \times z. \quad (24)$$

C. Training Objective

The loss function inspired by Leapfog [6] used to optimize both ASPILin and Lin is expressed as:

$$\mathcal{L} = \mathcal{L}_{\text{distance}} + \lambda \mathcal{L}_{\text{diversity}}, \quad (25)$$

$$\mathcal{L}_{\text{distance}} = \frac{1}{T_f} \min_{k=1}^K \sum_{t=1}^{T_f} \|\hat{y}_t^k - y_t\|_2, \quad (26)$$

$$\mathcal{L}_{\text{diversity}} = \frac{\sum_{k=1}^K \sum_{t=1}^{T_f} \|\hat{y}_t^k - y_t\|_2}{\sigma^2 K T_f} + \log \sigma^2. \quad (27)$$

We apply a winner-takes-all strategy to $\mathcal{L}_{\text{distance}}$, performing backpropagation only on the mode with the smallest deviation from the ground truth to prevent mode collapse. $\mathcal{L}_{\text{diversity}}$ with $\lambda = 0.02$ is designed to enhance the diversity of forecasted trajectories. The first component aligns variance with scene complexity, while the second component acts as a regularization factor, ensuring high variance across all predictions.

IV. EXPERIMENTS

A. Experimental Setup

1) *Datasets*: We train and evaluate our model on three interaction-rich datasets: the INTERACTION dataset [14], the highD dataset [15], and the CitySim dataset [16]. INTERACTION contains 398,409 and 107,269 sequences for ASPILin's training and validation and 413,548 and 111,493 sequences for Lin's training and validation. Each sequence is sampled at 10Hz, and the task is to use the past 1 second of sequence data to predict the next 3 seconds. In the case of highD, we split the dataset into 2,530,166 training sequences, 180,727 validation sequences, and 361,454 test sequences (7:1:2 ratio) and downsample the trajectories to 5Hz, following the data processing steps in PiP [25]. The prediction task involves using the past 3 seconds to predict the next 5 seconds. For CitySim, we use data from two no-signal scenarios, Intersection B and Roundabout A, with the training and validation split in an 8:2 ratio. The trajectory sampling rate for both scenarios is 30Hz, with the task being to predict the future 6 seconds trajectory based on the past 2 seconds. ASPILin and Lin use the same data for training and validation, including 61,185 training sequences and 15,164 validation sequences.

2) *Metrics*: For INTERACTION and CitySim, we forecast future trajectories for $K = 6$ modes and evaluate the model's performance using Minimum Average Displacement Error (minADE) and Minimum Final Displacement Error (minFDE), denoted as:

$$\text{minADE}_K = \frac{1}{T_f} \min_{k=1}^K \sum_{t=1}^{T_f} \|\hat{y}_t^k - y_t\|_2, \quad (28)$$

$$\text{minFDE}_K = \min_{k=1}^K \|\hat{y}_{T_f}^k - y_{T_f}\|_2. \quad (29)$$

For highD, we predict a deterministic unimodal trajectory and evaluate the model using Root Mean Square Error (RMSE), expressed as:

$$\text{RMSE} = \sqrt{\frac{1}{N T_f} \sum_{i=1}^N \sum_{t=1}^{T_f} \|\hat{y}_{t,i} - y_{t,i}\|_2^2}, \quad (30)$$

where N represents the total number of samples.

3) *Implementation Details*: The interaction module's range threshold \mathcal{D} is set to 30/200/45 meters for the INTERACTION/highD/CitySim dataset. Upper bound T is set to 30, and extra term ϵ is set to 1. In our proposed physics-related method, d_z and $d_{z'}$ are configured as 32 and 256, respectively, and the feed-forward module has a dimension of 256. For the spatiotemporal encoder, the Conv1D kernel size is set to 3, the output channels to 32, and the GRU's hidden layer dimension to 256. For the map encoder, we use the same settings as HEAT-I-R [2], where \mathcal{M} is a 400×250 grayscale map for each scene. For the three decoders, the hidden layers of $\text{MLP}_\mu(\cdot)$ and $\text{MLP}_\sigma(\cdot)$ are set to (256, 128), and the hidden layer of $\text{MLP}_z(\cdot)$ is set to (1024, 1024). The hidden layer and output dimension of linear transformations $\text{MLP}_{\sigma'}(\cdot)$ are set to (8, 16) and 32, respectively.

TABLE I
COMPARISON WITH MODELS ON THE INTERACTION VALIDATION SET

Model	Source	minADE ₆ ↓	minFDE ₆ ↓
HEAT-I-R [2] *	TITS 2022	0.19	0.66
ITRA [3]	ITSC 2021	0.17	0.49
GOHOME [13]	ICRA 2022	-	0.45
joint-StarNet [1]	IV 2022	0.13	0.38
DiPA [11]	RAL 2023	0.11	0.34
MB-SS-ASP [27]	IV 2023	0.10	0.30
SAN [28]	IV 2022	0.10	0.29
GMM-CVAE [23]	arXiv 2023	0.09	0.28
Lin *	-	0.18	0.67
ASPILin	-	0.08	0.27

*Model that only performs unimodal prediction.

TABLE II
COMPARISON WITH MODELS ON THE HIGHD TEST SET

Model	Source	RMSE↓				
		1s	2s	3s	4s	5s
CV	-	0.11	0.35	0.73	1.24	1.86
PiP [25]	ECCV 2020	0.17	0.52	1.05	1.76	2.63
MHA-LSTM [29]	TIV 2021	0.06	0.09	0.24	0.59	1.18
MMnTP [30]	RAL 2023	0.19	0.38	0.62	0.95	1.39
POVL [31]	ITSC 2023	0.12	0.18	0.22	0.53	1.15
VVF-TP [32]	ITSC 2023	0.12	0.24	0.41	0.66	0.98
iNATran [33]	TITS 2022	0.04	0.05	0.21	0.54	1.10
BAT [34]	AAAI 2023	0.08	0.14	0.20	0.44	0.62
Lin	-	<u>0.05</u>	<u>0.06</u>	<u>0.11</u>	<u>0.27</u>	<u>0.54</u>
ASPILin	-	<u>0.05</u>	0.05	0.08	0.21	0.42

ASPILin (3.5M/2.4M/5.8M parameters for the INTERACTION/highD/CitySim dataset) and Lin (2.5M/0.8M/2.9M parameters for the INTERACTION/highD/CitySim dataset) are trained on a single RTX-4090. We use AdamW as the optimizer, with a cosine annealing scheduler [26]. The initial settings for the learning rate, batch size, and training epochs are 1e-3, 64/128/32 for the INTERACTION/highD/CitySim dataset, and 40, respectively.

B. Comparison with State-of-the-art

The results on INTERACTION shown in Tab. I indicate that ASPILin achieves SOTA performance. Moreover, as a lightweight model that does not account for interactions, Lin still achieves the semblable performance as models

from the past 2-3 years, demonstrating the feasibility of our agent selection approach. The comparison results on highD are shown in Tab. II. Similar to some work [30], [31], we implemented a Constant Velocity (CV) model as a reference baseline. Interestingly, the performance after 1s exhibited by Lin exceeds that of SOTA methods, attributable to its superior CVAE architecture and loss functions. By comparison, ASPILin significantly reduces prediction error after 2s, highlighting the exceptional performance of our interaction modeling for long-term prediction.

C. Ablation Studies

1) *Components of the Interaction Module:* The ablation experiments for each component of the interaction module are shown in Tab III. The baseline configuration selects all agents within \mathcal{D} at time $t = 0$ as interacting agents and encodes their interactions using Transformer. Additionally, we introduced an extra simple agent selection method, which selects the four closest agents to verify the effectiveness of our method. An intuitive conclusion is that merely setting an upper limit on the number of interaction agents does not enhance model performance and may even reduce it. This is reasonable, as inappropriately narrowing the selection range will likely exclude genuinely interacting agents. However, switching the time window from current to all results in enhanced model performance, demonstrated across all three comparison sets (variants 2 and 3, 4 and 5, 6 and 7). Another interesting observation is that variants 2 and 3 are more significant than the other two groups. That’s because the four closest agents in interaction-dense scenarios may change at any moment, whereas four intent-matching agents are less likely to change over time. From comparisons in two other groups (variants 2 and 4, 3 and 5), we conclude that refining agent selection through lane usage can improve model performance, which provides valuable insights for future research. The last two comparisons (variants 4 and 6, 5 and 7) demonstrate that integrating physical interaction encoding is viable and advantageous, increasing the model’s interpretability.

2) *Four Types of Interacting Agents:* According to the results in Tab. IV, excluding any category of interacting agents results in some level of decline in model performance. Models excluding FF and FL, achieve the poorest

TABLE III
ABLATION EXPERIMENTS FOR EACH COMPONENT OF THE INTERACTION MODULE

Variant	Agent Selection		Time Windows		Interactions Encode		INTERACTION		CitySim	
	four lane-related	four closest	all	current	physics-related	attention	minADE ₆ ↓	minFDE ₆ ↓	minADE ₆ ↓	minFDE ₆ ↓
1				✓		✓	0.119	0.393	0.999	2.223
2		✓		✓		✓	0.117	0.392	1.010	2.253
3		✓	✓			✓	0.096	0.321	0.982	2.178
4	✓			✓		✓	0.097	0.331	0.973	2.164
5	✓		✓			✓	0.091	0.314	0.965	2.137
6	✓			✓	✓		0.088	0.295	0.959	2.124
7	✓		✓		✓		0.079	0.266	0.954	2.095

TABLE IV

ABLATION EXPERIMENTS FOR FOUR TYPES OF INTERACTING AGENTS

SL	FL	FF	ML	INTERACTION		CitySim	
				minADE ₆ ↓	minFDE ₆ ↓	minADE ₆ ↓	minFDE ₆ ↓
	✓	✓	✓	0.083	0.282	1.013	2.235
✓		✓	✓	0.080	0.269	1.025	2.307
✓	✓		✓	0.090	0.299	1.007	2.243
✓	✓	✓		0.085	0.271	0.962	2.104
✓	✓	✓	✓	0.079	0.266	0.954	2.095

performance on INTERACTION and CitySim, indicating that agents on the target agent’s future lane have a more significant impact on the target agent than other agents. Moreover, on the CitySim validation set, the prediction task is more sensitive to changes in interaction agents because of its 6-second prediction horizon.

3) *Different Lane Predictors*: Despite our clarification that the lane predictor based on classification is not practical for real-world applications, we implemented this approach to examine how the accuracy of future lane predictions affects model performance by a simple Random Forest (RF). The detailed experimental results are shown in Tab. V. Using raw data undoubtedly achieves the best performance. Interestingly, the classification- and regression-based models showed starkly different performances on the two datasets because the prediction tasks on the CitySim dataset are considerably more complex than those on INTERACTION, especially since interactions are not considered in both. What is not displayed in the table is that Lin’s ADE and FDE on the CitySim dataset are 2.809 and 7.785, respectively. Nevertheless, it maintains a high lane prediction accuracy, demonstrating that our comprehensive agent selection strategy is effective even for long-term prediction tasks with a simple model. Additionally, it can be observed that different methods have reduced the discrepancies in lane prediction in their final forecasts. This is because our agent selection is not entirely based on future lanes, and predicting an incorrect future lane may still lead to the same outcome due to other mismatched conditions.

TABLE V

ABLATION EXPERIMENTS FOR DIFFERENT LANE PREDICTORS

Dataset	Model	ACC(%)↓	minADE ₆ ↓	minFDE ₆ ↓
INTERACTION	Clf. (RF)	88.5	0.080	0.270
	Reg. (Lin)	97.9	0.079	0.266
	Raw Data	100	0.078	0.261
CitySim	Clf. (RF)	93.6	0.951	2.089
	Reg. (Lin)	89.5	0.954	2.095
	Raw Data	100	0.946	2.073

D. Qualitative Results

We present the qualitative results of ASPILin on the INTERACTION dataset. As illustrated in Fig. 3, our model can predict accurate, multi-modal vehicle trajectories in complex scenarios. Interestingly, ASPILin struggles more with predicting the precise trajectories of vehicles that are stationary or nearly so, which points to potential areas for future enhancements.

E. Inference Latency

TABLE VI

INFERENCE LATENCY FOR THREE DATASETS

Dataset	Model	LP	AS	TP	Total(ms)↓
INTERACTION	baseline	-	22.29	0.51	23.20
	ASPILin	1.00	8.52	0.24	9.76
CitySim	baseline	-	6.66	0.79	7.45
	ASPILin	0.99	6.53	0.26	7.78

We evaluate the inference latency of the entire prediction process, including Lane Prediction (LP), Agent Selection (AS), and Trajectory Prediction (TP) on INTERACTION and CitySim and compare it with the baseline (i.e., variant 1 in Tab. III). AS consumes most computational resources due to extensive data processing and conditional filtering. Even though ASPILin employs more criteria for meticulous agent selection, it remains more efficient than the baseline. In the INTERACTION dataset, up to 25 agents can be within 30 meters of the target agent, while in CitySim, there are a maximum of only 5 agents within 45 meters. This explains the discrepancies between ASPILin and the baseline in the

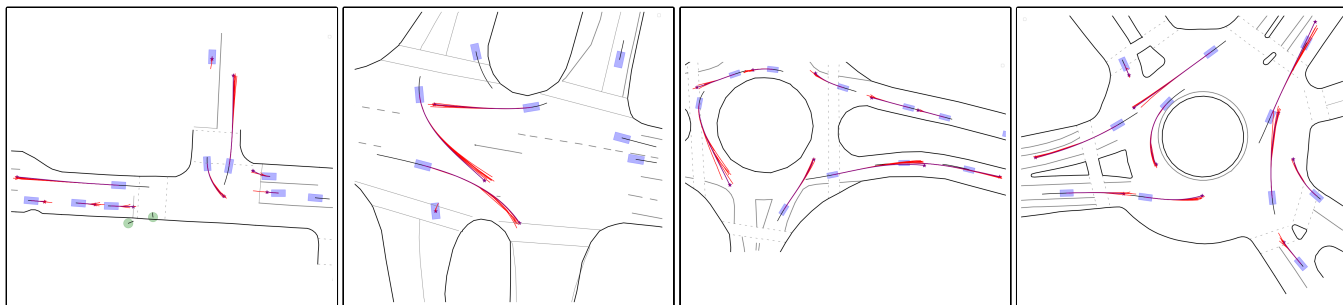


Fig. 3. Qualitative results on INTERACTION. Purple rectangles represent vehicles, while green circles denote pedestrians or cyclists. Past trajectories are shown with black lines, predicted future trajectories with red lines, and ground truth trajectories with purple lines, with endpoints marked distinctlyively.

two datasets. Results show that ASPILin possesses high inference efficiency, particularly in interaction-rich scenes. While its efficiency slightly underperforms the baseline in scenarios with low agent density, this is entirely acceptable.

V. CONCLUSION

In this work, we explored the possibility of enhancing interaction for trajectory prediction from two perspectives: (i) a lane-related method for a more detailed selection of interacting agents, and (ii) a physically-related interaction encoding method. We designed a model named ASPILin and conducted experiments on popular datasets. The results indicate that our approach significantly enhances interaction modeling and positively affects trajectory prediction, offering substantially increased interpretability over earlier methods.

REFERENCES

- [1] F. Janjos, M. Dolgov, and J. M. Zöllner, “Starnet: Joint action-space prediction with star graphs and implicit global-frame self-attention,” *2022 IEEE Intelligent Vehicles Symposium (IV)*, pp. 280–286, 2021.
- [2] X. Mo, Z. Huang, Y. Xing, and C. Lv, “Multi-agent trajectory prediction with heterogeneous edge-enhanced graph attention network,” *IEEE Transactions on Intelligent Transportation Systems*, vol. 23, pp. 9554–9567, 2022.
- [3] A. Scibior, V. Lioutas, D. Reda, P. Bateni, and F. D. Wood, “Imagining the road ahead: Multi-agent trajectory prediction via differentiable simulation,” *2021 IEEE International Intelligent Transportation Systems Conference (ITSC)*, pp. 720–725, 2021.
- [4] J. Gao, C. Sun, H. Zhao, Y. Shen, D. Anguelov, C. Li, and C. Schmid, “Vectornet: Encoding hd maps and agent dynamics from vectorized representation,” *2020 IEEE/CVF Conference on Computer Vision and Pattern Recognition (CVPR)*, pp. 11 522–11 530, 2020.
- [5] F. Janjos, M. Dolgov, and J. M. Zöllner, “Self-supervised action-space prediction for automated driving,” *2021 IEEE Intelligent Vehicles Symposium (IV)*, pp. 200–207, 2021.
- [6] W. Mao, C. Xu, Q. Zhu, S. Chen, and Y. Wang, “Leapfrog diffusion model for stochastic trajectory prediction,” *2023 IEEE/CVF Conference on Computer Vision and Pattern Recognition (CVPR)*, pp. 5517–5526, 2023.
- [7] Z. Zhou, L. Ye, J. Wang, K. Wu, and K. Lu, “Hivt: Hierarchical vector transformer for multi-agent motion prediction,” *2022 IEEE/CVF Conference on Computer Vision and Pattern Recognition (CVPR)*, pp. 8813–8823, 2022.
- [8] S. Shi, L. Jiang, D. Dai, and B. Schiele, “Mtr++: Multi-agent motion prediction with symmetric scene modeling and guided intention querying,” *IEEE Transactions on Pattern Analysis and Machine Intelligence*, vol. 46, pp. 3955–3971, 2023.
- [9] Z. Zhou, J. Wang, Y.-H. Li, and Y.-K. Huang, “Query-centric trajectory prediction,” *2023 IEEE/CVF Conference on Computer Vision and Pattern Recognition (CVPR)*, pp. 17 863–17 873, 2023.
- [10] Z. W. Pylyshyn and R. W. Storm, “Tracking multiple independent targets: evidence for a parallel tracking mechanism.” *Spatial vision*, vol. 3 3, pp. 179–97, 1988.
- [11] A. Knittel, M. Hawasly, S. V. Albrecht, J. Redford, and S. Ramamoorthy, “Dipa: Probabilistic multi-modal interactive prediction for autonomous driving,” *IEEE Robotics and Automation Letters*, vol. 8, pp. 4887–4894, 2022.
- [12] Q. Sun, X. Huang, J. Gu, B. C. Williams, and H. Zhao, “M2i: From factored marginal trajectory prediction to interactive prediction,” *2022 IEEE/CVF Conference on Computer Vision and Pattern Recognition (CVPR)*, pp. 6533–6542, 2022.
- [13] T. Gilles, S. Sabatini, D. V. Tsishkou, B. Stanculescu, and F. Moutarde, “Gohome: Graph-oriented heatmap output for future motion estimation,” *2022 International Conference on Robotics and Automation (ICRA)*, pp. 9107–9114, 2021.
- [14] W. Zhan, L. Sun, D. Wang, H. Shi, A. Clause, M. Naumann, J. Kümmerle, H. Königshof, C. Stiller, A. de La Fortelle, and M. Tomizuka, “Interaction dataset: An international, adversarial and cooperative motion dataset in interactive driving scenarios with semantic maps,” *ArXiv*, vol. abs/1910.03088, 2019.
- [15] R. Krajewski, J. Bock, L. Kloecker, and L. Eckstein, “The high dataset: A drone dataset of naturalistic vehicle trajectories on german highways for validation of highly automated driving systems,” *2018 21st International Conference on Intelligent Transportation Systems (ITSC)*, pp. 2118–2125, 2018.
- [16] O. Zheng, M. A. Abdel-Aty, L. Yue, A. Abdelraouf, Z. Wang, and N. Mahmoud, “Citysim: A drone-based vehicle trajectory dataset for safety oriented research and digital twins,” *ArXiv*, vol. abs/2208.11036, 2022.
- [17] J. Ngiam, V. Vasudevan, B. Caine, Z. Zhang, H.-T. L. Chiang, J. Ling, R. Roelofs, A. Bewley, C. Liu, A. Venugopal, D. J. Weiss, B. Sapp, Z. Chen, and J. Shlens, “Scene transformer: A unified architecture for predicting future trajectories of multiple agents,” in *International Conference on Learning Representations*, 2022.
- [18] M. Liu, H. Cheng, L. Chen, H. Broszio, J. Li, R. Zhao, M. Sester, and M. Y. Yang, “Laformer: Trajectory prediction for autonomous driving with lane-aware scene constraints,” *ArXiv*, vol. abs/2302.13933, 2023.
- [19] P. Bhattacharyya, C. Huang, and K. Czarnecki, “Ssl-lanes: Self-supervised learning for motion forecasting in autonomous driving,” *ArXiv*, vol. abs/2206.14116, 2022.
- [20] H. Zhao, J. Gao, T. Lan, C. Sun, B. Sapp, B. Varadarajan, Y. Shen, Y. Shen, Y. Chai, C. Schmid, C. Li, and D. Anguelov, “Tnt: Target-driven trajectory prediction,” in *Conference on Robot Learning*, 2020.
- [21] B. Varadarajan, A. S. Hefny, A. Srivastava, K. S. Refaat, N. Nayakanti, A. Cornman, K. M. Chen, B. Douillard, C. P. Lam, D. Anguelov, and B. Sapp, “Multipath++: Efficient information fusion and trajectory aggregation for behavior prediction,” *2022 International Conference on Robotics and Automation (ICRA)*, pp. 7814–7821, 2021.
- [22] A. Gupta, J. Johnson, L. Fei-Fei, S. Savarese, and A. Alahi, “Social gan: Socially acceptable trajectories with generative adversarial networks,” in *2018 IEEE/CVF Conference on Computer Vision and Pattern Recognition*, 2018, pp. 2255–2264.
- [23] F. Janjos, M. Hallgarten, A. Knittel, M. Dolgov, A. Zell, and J. M. Zöllner, “Conditional unscented autoencoders for trajectory prediction,” *ArXiv*, vol. abs/2310.19944, 2023.
- [24] S. Shleifer, J. Weston, and M. Ott, “Normformer: Improved transformer pretraining with extra normalization,” *ArXiv*, vol. abs/2110.09456, 2021.
- [25] H. Song, W. Ding, Y. Chen, S. Shen, M. Y. Wang, and Q. Chen, “Pip: Planning-informed trajectory prediction for autonomous driving,” in *European Conference on Computer Vision*, 2020.
- [26] I. Loshchilov and F. Hutter, “Sgdr: Stochastic gradient descent with warm restarts,” *arXiv: Learning*, 2016.
- [27] F. Janjos, M. Keller, M. Dolgov, and J. M. Zöllner, “Bridging the gap between multi-step and one-shot trajectory prediction via self-supervision,” *2023 IEEE Intelligent Vehicles Symposium (IV)*, pp. 1–8, 2023.
- [28] F. Janjos, M. Dolgov, M. Kuric, Y. Shen, and J. M. Zöllner, “San: Scene anchor networks for joint action-space prediction,” *2022 IEEE Intelligent Vehicles Symposium (IV)*, pp. 1751–1756, 2022.
- [29] K. Messaoud, I. Yahiaoui, A. Verroust-Blondet, and F. Nashashibi, “Attention based vehicle trajectory prediction,” *IEEE Transactions on Intelligent Vehicles*, vol. 6, pp. 175–185, 2020.
- [30] S. Mozaffari, M. A. Sormoli, K. Koufos, and M. Dianati, “Multimodal manoeuvre and trajectory prediction for automated driving on highways using transformer networks,” *IEEE Robotics and Automation Letters*, vol. 8, pp. 6123–6130, 2023.
- [31] S. Mozaffari, M. A. Sormoli, K. Koufos, G. Lee, and M. Dianati, “Trajectory prediction with observations of variable-length for motion planning in highway merging scenarios,” *2023 IEEE 26th International Conference on Intelligent Transportation Systems (ITSC)*, pp. 5633–5640, 2023.
- [32] M. A. Sormoli, A. Samadi, S. Mozaffari, K. Koufos, M. Dianati, and R. Woodman, “A novel deep neural network for trajectory prediction in automated vehicles using velocity vector field,” *2023 IEEE 26th International Conference on Intelligent Transportation Systems (ITSC)*, pp. 4003–4010, 2023.
- [33] X. Chen, H. Zhang, F. Zhao, Y. Cai, H. Wang, and Q. Ye, “Vehicle trajectory prediction based on intention-aware non-autoregressive transformer with multi-attention learning for internet of vehicles,” *IEEE Transactions on Instrumentation and Measurement*, vol. 71, pp. 1–12, 2022.
- [34] H. Liao, Z. Li, H. Shen, W. Zeng, D. Liao, G. Li, S. E. Li, and C. Xu, “Bat: Behavior-aware human-like trajectory prediction for autonomous driving,” in *AAAI Conference on Artificial Intelligence*, 2023.